AIAA JOURNAL
Vol. 36, No. 12, December 1998

Direct Measurement of Delta-Wing Vortex Circulation

H. Johari* and J. Moreira†
Worcester Polytechnic Institute, Worcester, Massachusetts 01609

The circulation around a closed path encompassing the primary vortex of stationary delta wings has been investigated through the use of a novel ultrasound technique. Ultrasonic pulses propagating in clockwise and counterclockwise directions enclosed a fixed path that was positioned perpendicular to the delta-wing root chord line. Circulation in the plane of the closed path then was determined from the transit-time difference between the clockwise and counterclockwise pulses. Half-delta wings with sweep angles of 60 and 70 deg were tested over a range of angles of attack up to 38 and 52 deg, respectively, and at chordwise distances of 35, 50, 65, and 80% from the wing apexes. Circulation increased monotonically with angle of attack for both sweep angles until it reached a maximum value, beyond which the total circulation decreased or remained nearly constant. The angle of attack associated with the maximum circulation is correlated with conditions resulting in feeding sheet interaction on the symmetry plane. At any angle of attack, circulation increased approximately linearly with increasing chordwise location as long as the feeding-sheet interaction was not present. Normalizing circulation by freestream velocity and local semispan collapsed the data at angles of attack prior to the interaction. The rate of circulation increase along the wing increased with angle of attack for both sweep angles. Vortex breakdown does not appear to have any direct influence on the total circulation of delta-wing vortices.

Introduction

THE flow pattern about delta wings is distinguished by a pair of longitudinal primary vortices. As the angle of attack of a delta wing increases, the boundary layer on the windward side gets separated over the leading edges. Shear layers formed in this manner roll up into the counter-rotating primary vortices on the leeward side of the wing.[1] The induced spanwise flow due to the primary vortices causes secondary separation on the wing surface, thus creating secondary vortices. As the angle of attack is increased, the primary vortices strengthen and result in a substantial lift increment beyond that predicted by attached-flow theory.[2]

Delta-wing performance has been thought to be limited by the phenomenon of vortex breakdown. Breakdown, or bursting, is marked by an abrupt expansion of the vortex core. There is a concurrent loss of axial and circumferential velocities in the flowfield, and these losses are accompanied by the transformation of the vortex core into a diffuse, turbulent vortex.[3] As a delta wing's angle of attack increases, the primary vortex burst location moves toward the wing apex. Numerous experiments have examined the effects of various parameters on vortex breakdown. The Reynolds number has proven to have only a slight effect[4]; breakdown is effectively independent of Reynolds numbers for values on the order of 10^5 and greater. It had been supposed that tunnel blockage effects could cause an effectively cambered wing that would delay breakdown. Tunnel blockage effects and support-structure interference also have been shown to cause minor deviation in the vortex burst location.[5] However, more relevant intrusions into the delta-wing vortices, such as the introduction of probes and disks, can considerably alter the burst location.[4,6]

Maximum lift of delta wings also has been correlated with vortex breakdown. For wing sweep angles less than 70 deg, maximum lift occurs approximately when the burst location reaches the apex, whereas for higher sweep angles, maximum lift is observed when the vortex bursts in the vicinity of the trailing edge. To shed light on the influence of burst location on delta-wing lift and stall, both the variation of the primary vortex circulation $\Gamma(x)$ along the chord and the vortex core distance above the wing z_c are necessary because the suction on the wing surface beneath the vortex core scales approximately with $(\Gamma/z_c)^2$. Flow visualization has been used in a number of experiments[4,7,8] to measure the vortex trajectory $z_c(x)$. However, circulation of the primary vortex is much more difficult to measure, and only a few attempts[9–11] have been made to quantify Γ under certain conditions. Circulation has been postulated to grow approximately linearly with increasing distance from the wing apex, upstream of the burst location.[9] Furthermore, the rate of circulation growth reportedly decreases aft of the midchord location; this has been attributed to the adverse pressure gradient imposed by the wing's trailing edge.[9]

The present study was undertaken to quantify the circulation of the delta-wing primary vortices and to examine the variation of circulation with angle of attack and chordwise location for wing sweep angles of 60 and 70 deg. These two sweep angles were chosen because they represent the canonical behavior of low- and high-sweep-angle delta wings. Moreover, the aerodynamic properties of 60- and 70-deg delta wings, which have been studied extensively in the past, are well established. The following fundamental questions can be answered by the measurements of delta-wing vortex circulation over a broad range of parameters:

1) Does the total circulation increase monotonically with the angle of attack even at high α?

2) How does vortex breakdown affect the total circulation above delta wings?

3) Does circulation scale with the local semispan for all angles of attack and chordwise locations? (That is, is the conical flow model a good approximation for delta-wing primary vortices?)

The search for a reliable and nonintrusive circulation measurement method led us to the employment of a novel ultrasound technique. This technique, which provides a direct measurement of circulation, is described in the next section. Comparisons of directly measured data were made with circulation values obtained from velocity field data[9–11] and a model based on Sychev's parameter[12] and Hemsch–Luckring[13] scaling.

Ultrasound Approach

Vortex strength can be quantified by measuring the circulation about a closed path that contains the vortex. Circulation is obtained by integrating the local velocity along the closed path or by integrating the vorticity component perpendicular to the plane of the closed path contained within the closed path. Thus, the velocity (or vorticity) field information in the plane of the closed path is required for the calculation of circulation. Velocity vectors in a flowfield can be determined via traditional methods such as hot-wire or laser

Presented as Paper 97-0743 at the AIAA 35th Aerospace Sciences Meeting, Reno, NV, Jan. 6–9, 1997; received Feb. 24, 1998; revision received Aug. 10, 1998; accepted for publication Aug. 19, 1998.

*Associate Professor, Mechanical Engineering Department. Senior Member AIAA.

†Graduate Student, Mechanical Engineering Department.

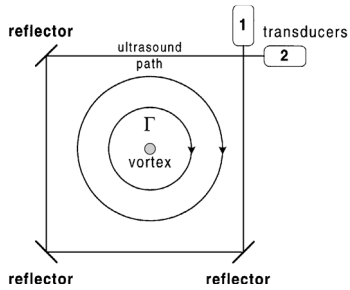

Fig. 1 Schematic of generic ultrasound system for direct measurement of circulation.

Doppler anemometry (LDA). Large amounts of data are needed for adequate resolution of spatial distributions, and therefore much testing time can be required. The wandering motion of free vortices also may undermine the stationary-flow requirement, which justifies the time averaging of anemometry data. The use of hot-wire probes circumvents the seeding difficulties associated with LDA and provides adequate data upstream of the vortex burst location, yet the reliability of hot-wire data from the burst vicinity and the flow farther downstream can be questionable because burst vortices are quite sensitive to physical intrusions. Particle image velocimetry (PIV) uses high-resolution video or photographic equipment and a pulsed-laser light sheet to measure an array of near-instantaneous velocity vectors in a two-dimensional section of flow. This method can reveal spatial flow structures as well as aggregate measures such as flow rate and circulation.[14] However, the complexity and expense of PIV systems can preclude their use under certain circumstances. Readily obtainable circulation values are quite advantageous from a practical standpoint because circulation can reveal loading distribution and other similarly important parameters.

Schmidt[15] first raised the possibility of using ultrasound in connection with circulation measurements of aerodynamic devices in wind-tunnel tests. The ultrasound method relies on the fact that the speed of sound traveling through a fluid in motion is increased or decreased by the component of fluid velocity along the sound path. In our efforts[16] we have developed a method that is based on Schmidt's work and avoids the assumption of free vortex velocity profile used by Schmidt. The method utilizes a pair of ultrasonic transducers, which can act as both transmitters and receivers, to create pulses that travel in a continuous closed path around the vortex. The closed path is attained through redirection of the ultrasonic pulses by reflectors placed within the flow, as shown in Fig. 1. The reflection follows Snell's law because narrow, high-frequency ultrasound pulses behave essentially as geometric rays with divergence angles of a few degrees. The time of travel between the transmitter and the receiver is measured accurately for pulses traveling in the direction of vortex rotation and against it. As will be shown later, the difference between the two travel times is linearly proportional to the circulation contained within the closed path. Improvements in ultrasound measurement technology have enabled measurement of time differences on the order of a few nanoseconds; accurate circulation measurements thus can be made in laboratory-scale experiments.

The ultrasonic circulation measurement technique requires the determination of the transit time of ultrasonic pulses traveling in the sense of vortex rotation (t_{cw}) and opposite to it (t_{ccw}); see Fig. 1. Then

$$t_{cw} = \oint \frac{\mathrm{d}l}{a + V(l)}, \qquad t_{ccw} = \oint \frac{\mathrm{d}l}{a - V(l)} \tag{1}$$

where $V(l)$ is the local fluid velocity component along the closed path, a is the sound speed, and $\mathrm{d}l$ is the line element along the closed path. By taking the difference between these two transit times, an expression for the line integral of velocity along the closed path can be obtained as follows:

$$\Delta t = t_{ccw} - t_{cw} = 2 \oint \frac{V(l)/a^2}{1 - (V/a)^2}\mathrm{d}l \cong \frac{2}{a^2} \oint V(l)\mathrm{d}l \tag{2}$$

The final expression on the right-hand side holds as long as the ratio V/a remains small (roughly less than 0.1). This condition is invariably satisfied for low-speed air flows, especially because V is the velocity component along the closed sound path and not necessarily the freestream velocity. Further, by propagating ultrasound pulses in both directions along the same path within a low-speed flow ($V \ll a$), possible complications resulting from the sound speed variation in the closed path are effectively nullified.[17] Because circulation Γ is the line integral of velocity around a closed path, this transit-time-difference relation simplifies to

$$\Gamma \equiv \oint V(l)\mathrm{d}l = \frac{1}{2}a^2 \Delta t \tag{3}$$

This expression allows for the direct computation of circulation from the accurately measurable transit time difference Δt and the speed of sound. This method of circulation measurement has two benefits over the ultrasound method developed by Schmidt.[15] The precise location of the vortex core relative to the ultrasonic path is not needed. Moreover, a priori knowledge of the vorticity distribution or the induced velocity behavior is not assumed in the present closed-path scheme. Further details about the ultrasound method and its accuracy and reliability can be found in Ref. 16.

Applying the ultrasound method to delta-wing flow has several clear advantages. First, it is nonintrusive with respect to the flow immediately about the leeward side of the delta wing. Second, the location of the vortex core in relation to the ultrasonic path is not particularly relevant as long as the vortex is within the closed path. The vortex core is free to move within the path without affecting the measured Δt or Γ. Third, the details of the velocity or vorticity distributions are not required. Note that circulation of delta-wing vortices depends on the geometry and area of the integration contour. For circular paths centered on the vortex core, circulation varies with the radial distance until a maximum value is reached. The current ultrasound technique does not permit formation of circular paths. Therefore, a large rectangular ultrasound path was utilized to measure the total circulation; i.e., the integration contour enclosed all vorticity-containing regions.

Experimental Details

Apparatus

The experiments were conducted in Worcester Polytechnic Institute's low-speed wind tunnel, which has a test section of 61×46 cm cross-sectional area. The freestream velocity U_o was held constant at 11.2 m/s, and the measured turbulence in the tunnel was 0.7%. Flat-plate wings with sweep angles of $\Lambda = 60$ and 70 deg in a half-delta configuration were chosen for the investigation because only a single primary vortex would be present on the windward side. The wings had a (nominal) root chord length c of 25.4 cm, resulting in a chord Reynolds number ($U_o c/\nu$) of 1.9×10^5. This chord length was chosen as a compromise that would yield significant vortex circulation without causing excessive tunnel blockage. The area blockage varied from 2.7 to 7% across the angle-of-attack range and averaged approximately 4%.

Eight half-delta wings of 0.9% thickness ratio were manufactured from 2.3-mm-thick T304 stainless steel. Thinness was mandated by previous experimental observations that show the thickness ratio to be an important factor in determining primary vortex behavior.[5,18] The windward side of the leading edge of each wing was beveled at 40 deg to fix the separation point of the shear layers. The necessity for multiple wings per sweep angle was incurred by transducer geometry; the two 19-mm-diam ultrasonic transducers dictated that a half-delta wing be made for every chordwise measurement station. Tolerances on all parts constructed for the present study were 0.01 mm. Therefore, all four wings of each sweep angle appeared identical to the flow; this assessment is supported by forthcoming burst measurement data.

To avoid excessively thick boundary layers on the half-delta wings, a raised (false) floor[19] with an imbedded turntable was designed and installed in the wind tunnel. The 41-cm-diam turntable and raised floor were constructed from 6.35-mm-thick aluminum. The turntable was designed to lock the delta wings into angles of attack ranging from 0 to 52 deg (in 2-deg increments) and was capable of being adjusted about 0 deg for maximum accuracy. Angles of attack were accurate to within ± 0.02 deg as determined from worst-case machining tolerances. The wings were fully adjustable within the turntable such that sweep-angle accuracy, as installed, was approximately ± 0.1 deg. The raised floor extended only 5.1 cm from

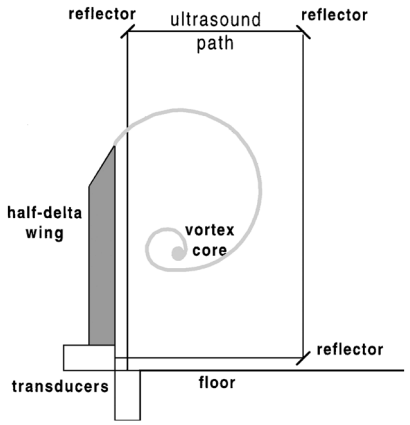

Fig. 2 Ultrasound system configuration about a half-delta wing.

the upstream end of the turntable, thereby minimizing the buildup of boundary-layer thickness at the wing measuring locations. One of the three ultrasound reflectors was carried on the turntable, and the two others were suspended from the top of the wind tunnel on a rotating assembly.

The ultrasound path employed in the study is shown in Fig. 2; it was a rectangle of 305×203 mm, which was always normal to the root chord line of the half-delta wings. These dimensions were greater than the span of half-delta wings used. The large integration contour encompassed all of the vorticity-containing regions above the delta wings, and the measured circulations are expected to be the maximum or total value at each chordwise station. Because the path extended to the undisturbed freestream flow, the measured circulation should be independent of the path for the large contour utilized in the setup.

Two transducers were used, and each behaved alternately as an emitter and a receiver. Thus, one transducer began a measuring cycle by emitting specially tailored ultrasonic pulses while the other acted as a receiver. After completing the travel-time measurement in this cycle, the second transducer emitted pulses in the opposite direction along the same path; this second cycle of pulses was received by the original emitter. Circulation then was found directly by computing the time difference required for each pulse to travel the closed path. The operating frequency of the transducers was 100 kHz in the study; this is above the wind-tunnel noise bandwidth, and thus no acoustic interference was expected. Because reflectors must have significantly higher acoustic impedance than that of the fluid through which the ultrasound propagates, square stainless-steel plates were employed in this capacity.

A commercial ultrasonic flowmeter was used for controlling the transducers as well as measuring the transit-time differences. Although ultrasonic flowmeters can measure time differences as small as a few nanoseconds, a minimum Δt of 50 ns was evidenced with the 1-m path length of the present setup. This uncertainty in the Δt measurements translates to an uncertainty of $\pm 0.003\ \mathrm{m}^2/\mathrm{s}$ for circulation in air at room temperature. At 2-deg angle of attack, this uncertainty amounts to an error of about 5%, whereas the error is only 0.4% at the highest measured circulation value. These relative uncertainties are less than the measured standard deviations of circulation data at all measurement stations.

Recall that values of V/a (the velocity component along the ultrasonic path divided by the speed of sound) of approximately less than 0.1 are necessary for circulation to be linearly proportional to transit-time difference. The speed of sound was calculated from the perfect-gas relation $a = \sqrt{(\gamma RT)}$ because the measured humidity in the laboratory was sufficiently low. The maximum tangential-velocity component around the primary vortices can reach as much as $2U_o$ (Ref. 9). In the present study, the freestream velocity U_o was held constant at 11.2 m/s. This yields, even in a worst-case scenario, a value of about 0.06 for V/a; note that this is well within the 0.1 limitation. Typical values of V/a along the ultrasound path were substantially smaller than 0.06.

Both 60- and 70-deg sweep-angle half-delta wings were tested at 35, 50, 65, and 80% of the root chord from the apex. For each measurement location, angle of attack α was varied in 2-deg increments from 2 to 38 deg for the 60-deg delta wings and from 2 to 52 deg for the 70-deg delta wings. Measurement locations aft of 0.80c were not considered because of concern over the possible effects of the trailing edge; measuring stations closer to the apex than 0.35c were not considered because of the relatively large size of the transducers with respect to the local semispan. Near-apex measurements would have resulted in incomplete enclosure of the vortex core by the ultrasound path. Mean circulation and standard deviation were calculated for each data set, with sets consisting typically of 100 points gathered at each measurement station and angle of attack.

Verifications

To ascertain that the half-wing models were identical to each other and produced primary vortices similar to those in other studies, smoke flow visualization experiments were performed. Vortex burst location was measured visually for both 60- and 70-deg sweep angles. Both bubble and spiral vortex bursts were observed, and no specific trends regarding the occurrence of the breakdown type with α or wing sweep angle could be deduced. The observed burst location x_b/c, plotted in Fig. 3, corroborated well with the ranges corresponding to other measurements from Refs. 4, 18, 20, and 21 for the 60-deg wing and from Refs. 4–6, 20, and 21 for the 70-deg wing. The fluctuations of the burst point were estimated visually to be on the order of 5% of chord. Note that data from two of the current 70-deg sweep-angle wings with the ultrasound transducers placed at 0.35c and 0.80c are presented in Fig. 3b. No significant deviation of one from the other is evident once the burst location uncertainty is taken into account. Thus, the primary vortices generated by the present half-wing models have burst location characteristics similar to those of full delta wings studied previously.

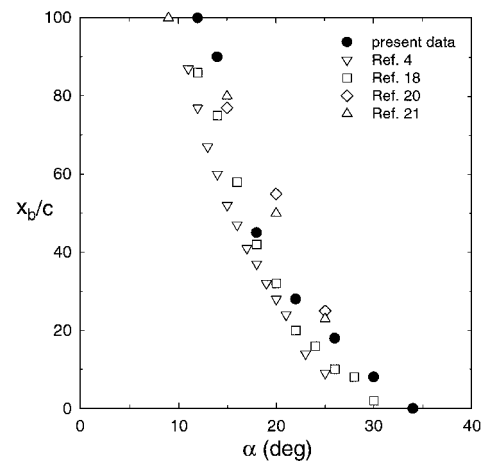

a) 60-deg sweep delta wing

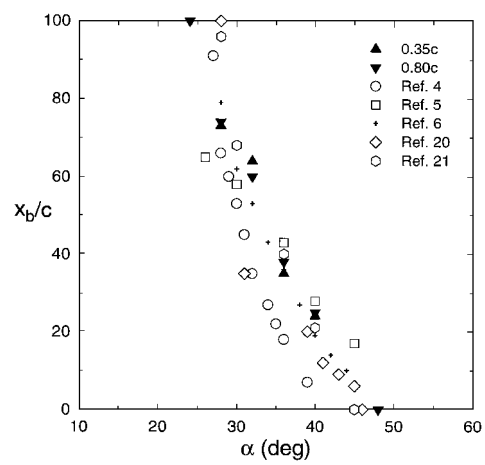

b) 70-deg sweep delta wing

Fig. 3 Primary vortex burst location as a function of angle of attack. The half-delta wings with the transducers placed at 0.35c and 0.80c stations are represented by ▲ and ▼ symbols, respectively.

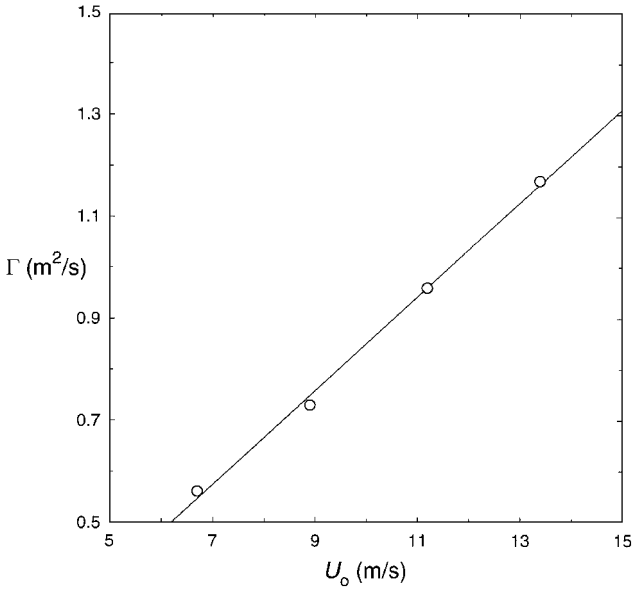

Fig. 4 Dependence of circulation at the 0.65*c* station on the freestream velocity for a 70-deg sweep delta wing at 26-deg angle of attack.

To confirm the linearity of total circulation with freestream velocity, the variation of circulation, measured as U_o, was increased from 6.7 to 13.4 m/s. The data obtained with the 70-deg delta wing at an angle of attack of 26 deg and chordwise location of 0.65*c* are shown in Fig. 4. At this angle of attack, the burst location is in the vicinity of the trailing edge and the measurements at 0.65*c* correspond to a well-formed, unburst vortex. As expected, the data indicate a linear increase in circulation with increasing freestream velocity.

The distribution of the measured ultrasound time differences $\Delta t (\propto \Gamma)$ was examined under various conditions to obtain an understanding of the spread of data about the mean values. Although both 60- and 70-deg delta wings displayed similar characteristics under comparable conditions, the data from the 70-deg wing generally yielded larger standard deviations and were somewhat more susceptible to the presence of burst in the vicinity of the measurement plane. Therefore, four histograms of Δt data for the 70-deg delta wing are presented in Fig. 5. The first three histograms pertain to the 0.80*c* location: Fig. 5a corresponds to an angle of attack of 14 deg, where the vortex does not burst over the wing; Fig. 5b shows data from the 28-deg angle of attack, where the burst location is approximately at the measurement plane; and the data of Fig. 5c were taken at 52-deg angle of attack with the burst location at the apex. The means and standard deviations at these conditions are 11.15 ($\pm$0.58), 24.58 ($\pm$0.65), and 27.62 ($\pm$0.88) μs, respectively. Even though the standard deviations increase as the burst location moves ahead of the measurement location, the magnitudes relative to the mean do not change appreciably. Little effect from the burst location on the character of the histograms can be observed. At most angles of attack and chordwise measurement stations, data were very cohesive and the standard deviation of Δt data increased only slightly following vortex breakdown.

As the measurement station is brought nearer to the apex, data sets begin to show larger spreads with burst proximity and with approach of the burst location to the apex. The histogram in Fig. 5d is included as a worst-case example from the 0.50*c* measurement station at $\alpha = 50$ deg with the burst location at the apex of the 70-deg wing. The mean value of Δt is 15.29 μs with a standard deviation of 2.7 μs. The vast majority of data sets exhibited more favorable behavior and more closely reflect those of the first three histograms. It is suspected that the larger standard deviations of burst vortices at the near-apex station is primarily due to the wandering of the burst vortex and the possible interaction of vorticity-containing regions with the symmetry plane or the ultrasound path.

Results and Discussion

The variation of measured circulation, normalized by the freestream velocity and root chord length, with angle of attack is shown in Figs. 6 and 7, respectively, for the 60- and 70-deg sweep-angle

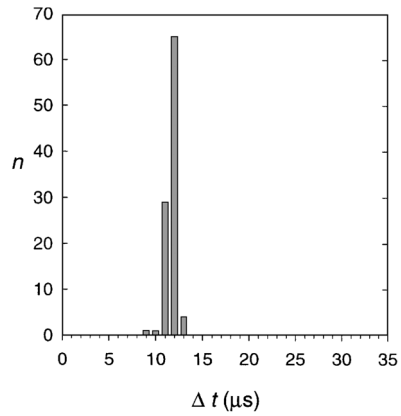

a) $x/c = 0.80c$, $\alpha = 14$ deg, $\overline{\Delta t} = 11.2$ μs, $\sigma = 0.6$ μs

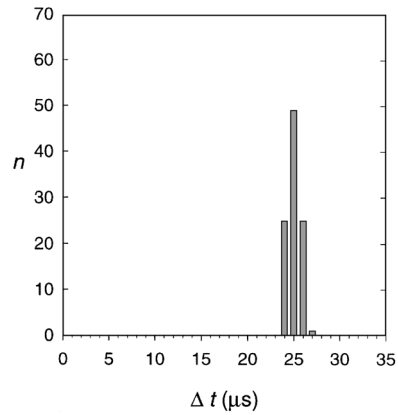

b) $x/c = 0.80c$, $\alpha = 28$ deg, $\overline{\Delta t} = 24.6$ μs, $\sigma = 0.7$ μs

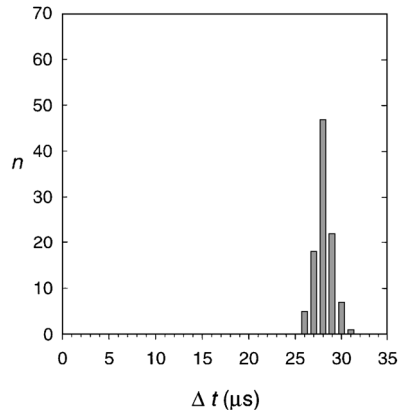

c) $x/c = 0.80c$, $\alpha = 52$ deg, $\overline{\Delta t} = 27.6$ μs, $\sigma = 0.9$ μs

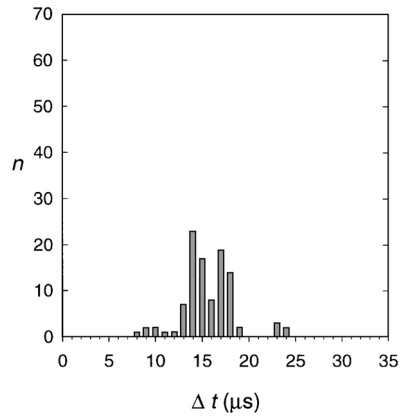

d) $x/c = 0.50c$, $\alpha = 50$ deg, $\overline{\Delta t} = 15.3$ μs, $\sigma = 2.7$ μs

Fig. 5 Histograms of measured time differences for a 70-deg sweep delta wing.

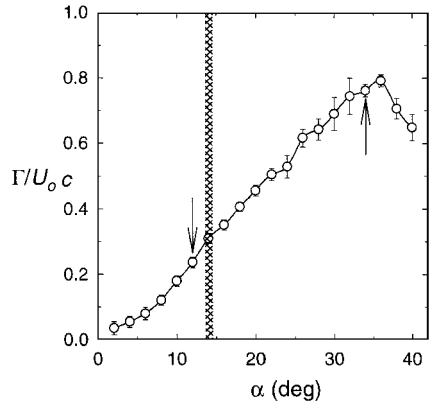

a) $x/c = 0.80$

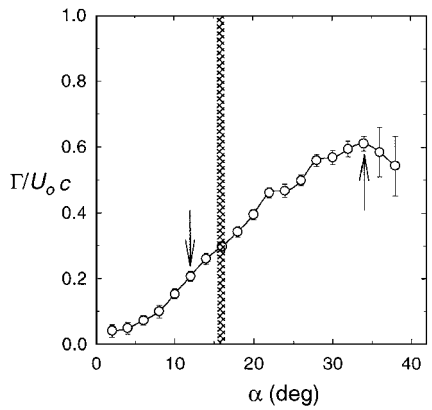

b) $x/c = 0.65$

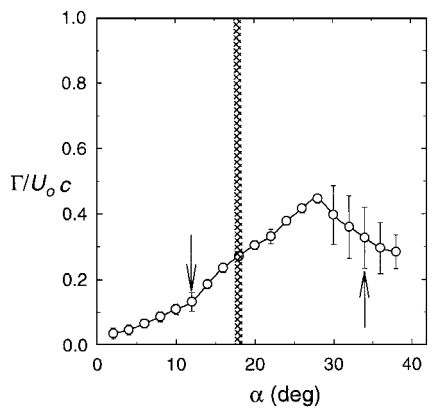

c) $x/c = 0.50$

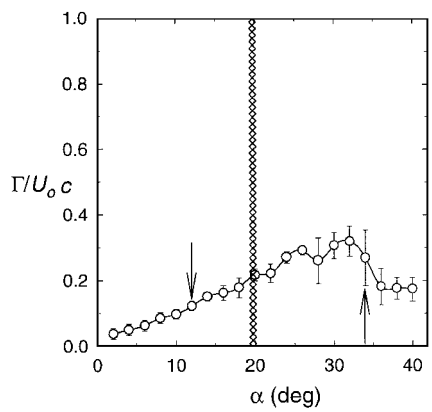

d) $x/c = 0.35$

Fig. 6 Variation of normalized circulation with angle of attack for 60-deg sweep delta wing. The arrows indicate the angles at which the burst location is at the trailing edge and apex. The cross-hatched line denotes the approximate angle of attack at which the burst location is at the measurement station.

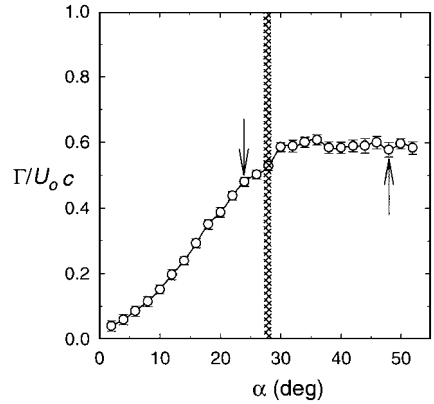

a) $x/c = 0.80$

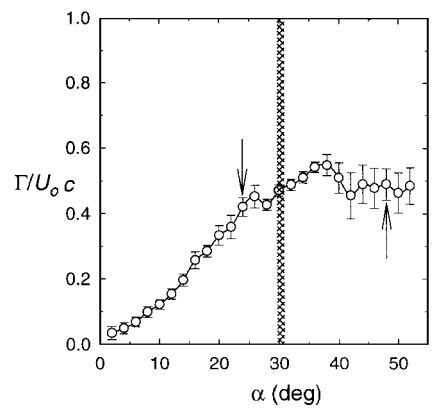

b) $x/c = 0.65$

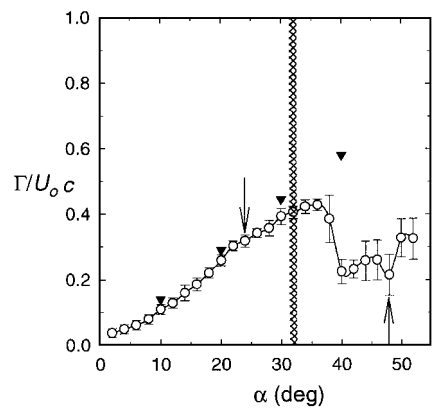

c) $x/c = 0.50$

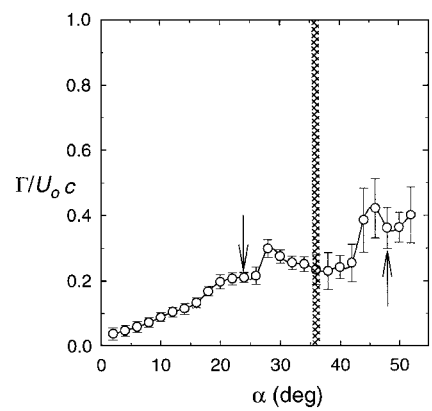

d) $x/c = 0.35$

Fig. 7 Variation of normalized circulation with angle of attack for 70-deg sweep delta wing. The arrows indicate the angles at which the burst location is at the trailing edge and apex. The cross-hatched line denotes the approximate angle of attack at which the burst location is at the measurement station.

delta wings. Each plot represents data at one of the four measurement stations along the chord, $x/c = 0.80$, 0.65, 0.50, and 0.35. Error bars indicate ± 1 standard deviation of the measured data. Note that the standard deviations are generally much larger than the uncertainty of the ultrasound system. The arrows mark the angles of attack at which the vortex breakdown is at the apex and the trailing edge of the wing, and the cross-hatched line in each figure denotes the angle of attack at which the vortex bursts at the measurement station. Recall that the breakdown location fluctuates considerably, and these markings therefore should be interpreted as approximate indicators.

The normalized circulation increases with angle of attack at all measurement stations for the 60-deg delta wing until a maximum is reached. The total circulation then decreases as α is increased further. The error bars are generally small and become significant only for angles of attack where circulation has started to decline. As expected, at any angle of attack the total circulation increases as the measurement station is moved toward the trailing edge. This is a result of the continuous accumulation of vorticity from the separated shear layer into the vortex core. The dependence of circulation on chordwise location is discussed in more detail later.

The presence of vortex breakdown in the vicinity of the measurement station can be assessed from these plots as well. As the breakdown crosses the trailing edge, no modification of the circulation at any of the four measurement stations is observed. The breakdown is not expected to affect the vortex at locations farther upstream. Even when the breakdown is at the measurement station, no change in the characteristics of the curves in Figs. 6 and 7 is observed, and total circulation continues to increase with α. Moreover, the error bars remain relatively unchanged by the appearance of the breakdown. Although the vortex structure is modified appreciably by the breakdown, the total circulation of the primary vortex stays the same. The arrival of the burst location at the apex of the 60-deg wing appears to be correlated with the reduction in the vortex circulation. However, the circulation decrease is not necessarily a direct consequence of the breakdown occurring at the apex. The reasons for the onset of circulation decline are presented later.

The dependence of circulation on α is shown in the plots of Fig. 7 for the 70-deg delta wing. Normalized circulation increases in a similar fashion at small angles of attack and at all four measurement stations. Again, arrival of the burst location at the measurement station does not appear to notably affect the total circulation. The major difference between the data of 60- and 70-deg sweep-angle wings is at the higher angles of attack; the circulation of the 70-deg wing became nearly constant, whereas the 60-deg wing data exhibited distinct circulation declines. The data for the $0.50c$ station of the 70-deg wing do indicate a decrease in circulation beyond $\alpha =$ 36 deg.

There are four data points in Fig. 7c from the study of Payne,[11] as reported in Ref. 9, where the circulation of the primary vortex was computed for a 70-deg delta wing at $x/c = 0.50$. The circulation was calculated from velocity field surveys carried out by a seven-hole probe. The reported values were computed from the largest circular contours investigated. The first three of these data points correspond to preburst conditions, whereas the fourth one at $\alpha = 40$ deg comes from a burst vortex. The first three data points are quite close (within 10%) to the current measurements. The postburst data point of Payne is significantly greater than our data. The discrepancy is possibly due to the presence of the intrusive seven-hole probe in an unsteady postburst vortex. Alternatively, the differences between the ultrasound path and the integration contour of Ref. 11 may produce the discrepancy.

The dependence of circulation on the chordwise location along the wing is shown in Fig. 8 for angles of attack of 12, 20, 28, and 36 deg. These angles of attack were chosen to observe the effects of breakdown location on the total circulation variation along the chord line. Furthermore, hot-wire and LDV measurements of the flowfield around the 70-deg delta wing are available from Refs. 9 and 10 for 20- and 28-deg angles of attack, respectively, at specific locations along the chord. At $\alpha = 12$ deg (Fig. 8a), the burst location is downstream of the trailing edge and circulation increases linearly with x/c for both 60- and 70-deg delta wings. As expected, the normalized circulation of the 60-deg wing is greater than that of the 70-deg

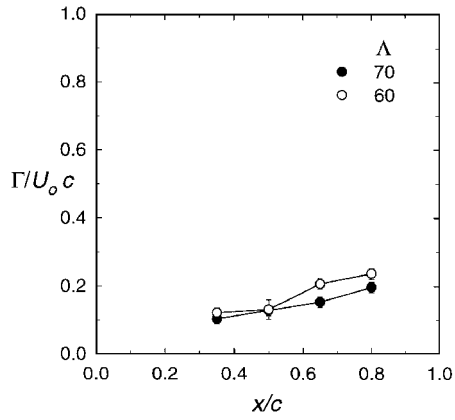

a) $\alpha = 12$ deg

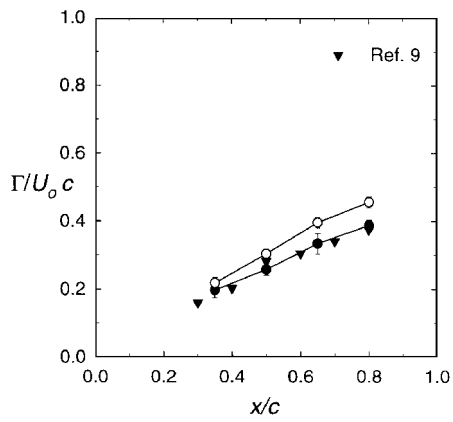

b) $\alpha = 20$ deg

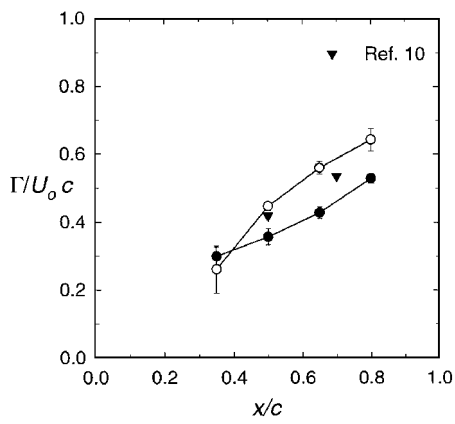

c) $\alpha = 28$ deg

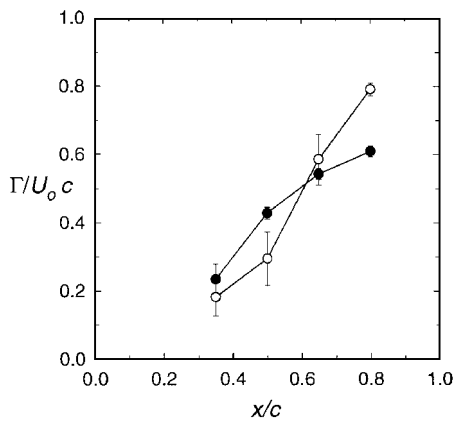

d) $\alpha = 36$ deg

Fig. 8 Dependence of normalized circulation on the axial location along the root chord. The open and filled symbols refer to 60- and 70-deg sweep delta wings, respectively.

wing because of the larger wing span of the 60-deg wing. The rate of increase in circulation is also larger for the 60-deg wing than for the 70-deg wing.

The case of $\alpha = 20$ deg is illustrated in Fig. 8b. The burst location is at $0.35c$ for the 60-deg wing, whereas the vortex does not break down over the 70-deg wing. Thus, all of the 60-deg wing data in Fig. 8b pertain to the burst portion of the vortex. Again, circulation increases linearly with x/c for the measured range, and the circulation values for the 60-deg wing are consistently larger than those for the 70-deg wing. The total circulation for a 75-deg delta wing, obtained by Visser and Nelson[9] from the integration of hot-wire measurements, also is included in Fig. 8b. The integration contour of Ref. 9 was a circular path centered on the vortex core. The largest measurements at the farthest radial distance are shown in Fig. 8b. These data fall slightly below current 70-deg wing data. It is expected that the 75-deg wing data should be less than those for the 70-deg wing because of its smaller span.

The variation of circulation with x/c at 28-deg angle of attack is shown in Fig. 8c, where the LDV measurements of Roos and Kegelman[10] for a sweep angle of 70 deg at locations of $0.5c$ and $0.7c$ also are included. At this angle of attack, the burst location is at $0.8c$ for the 70-deg wing and at $0.1c$ for the 60-deg wing. Even though the dependence of circulation on x/c still can be considered linear for the 70-deg wing, the 60-deg wing exhibits a departure from linearity. It is thought that this deviation is due to the observed reductions in the circulation (see Fig. 6) and not necessarily a result of the burst location approaching the wing apex. Note that the LDV data are somewhat greater than the present measurements. A possible reason is the difference in the integration contour of Ref. 10 and the ultrasound path used here.

The data in Fig. 8d refer to an angle of attack of 36 deg, where the burst location is at the apex for the 60-deg wing and at $0.35c$ for the 70-deg wing. Hence, all of the data in Fig. 8d come from burst portions of the vortex. Two aspects of this plot are noteworthy. First, dependence of circulation on x/c cannot be classified as linear for the 70-deg wing, and the data for $x/c \leq 0.6$ of the 60-deg wing fall below those of the 70-deg wing, in contrast to the data at smaller angles of attack. The previously noted reduction in circulation for the 60-deg wing at this relatively high angle of attack is the cause of the latter observation. The significant increases in the error bars for the 60-deg wing data are also noteworthy.

Considering the data in Fig. 8, one concludes that total circulation increases linearly with x/c as long as the burst location is downstream of the measurement location. The rate of increase in circulation $d\Gamma/dx$ increases with angle of attack and apex half-angle ε ($=90 \text{ deg} - \Lambda$). The linear dependence of circulation on x/c disappears when the angle of attack increases beyond a certain value for both sweep-angle delta wings examined. Our data did not exhibit a loss of total circulation as the burst location moved across the length of the vortex for the 60- and 70-deg delta wings; this contrasts with the seven-hole-probe data of Payne,[11] presented in Ref. 9, for an 85-deg sweep delta wing. Also, once the circulation increase with α is halted for the 60-deg wing, the normalized circulation $\Gamma/U_o c$ values for the 70-deg wing become greater than those of the 60-deg wing.

There are several concerns that need to be addressed at this point. They are the presence of secondary vortices beneath the primary vortices, the boundary layer on the false floor, and the reduction of total circulation at high angles of attack. The boundary layer on delta wings induced by the rotational motions of the primary vortex separates and forms a secondary vortex of opposite sign from the primary vortex. A potential difficulty concerns the current acoustic technique, which integrates all vorticity contained within the ultrasound path. If the secondary vortex were included within the ultrasound path, the measured circulation would be the net value for the primary minus the secondary vortex. The negative vorticity of the secondary vortex is not trivial and can amount to a circulation as much as 10–15% of the positive circulation of the primary vortex at midchord on a 75-deg wing at $\alpha = 20$ deg, as measured by Visser and Nelson.[9] The centerline of the transducers was placed approximately 1 cm away from the wing surface and the false floor. Thus, vorticity falling closer than 1 cm to the wing surface would not be measured by the acoustic system.

The hot-wire measurements of Ref. 9 show the distribution of axial vorticity at midchord on a 75-deg delta wing. The majority of negative vorticity falls below $0.2s$, where s is the local semispan. The measurements of Verhaagen and van Ransbeeck[22] indicate the negative vorticity to be within $0.1s$ from the wing surface on a 76-deg wing at a Reynolds number of a few million. If it is assumed that the extent of the negative vorticity scales with the local semispan for the 60- and 70-deg delta wings at all measurement stations, the conditions under which the secondary vortex would interfere with the ultrasound measurements can be estimated for the current setup. In fact, the farthest measurement station on the 70-deg wing and all four stations on the 60-deg wing could be affected to some extent in this manner. Then our measurements at the aforementioned stations could be less than the circulation associated with the primary vortex alone by as much as 15%.

An interesting aspect of the secondary vorticity observed in the data of Ref. 9 is the nearly constant circulation of secondary vortex along the chord, at least between $0.2c$ and $0.9c$, and at angles of attack of 20 and 30 deg. Therefore, the inclusion of secondary vorticity in our data can be approximated as a bias error of a constant fraction of the measurements for the 60-deg delta wing. The inclusion of negative-signed vorticity in our ultrasound path is perhaps one of the reasons for the consistently greater circulation values cited in Refs. 9 and 10.

The other possible adverse effect of installation on the measurements stems from the boundary layer on the floor supporting the half-wing. Because of the relatively low freestream velocity, the boundary layer is expected to be laminar. The boundary-layer thickness at the farthest measurement station of $0.8c$ was estimated to be 3 mm. With the centerline of ultrasound transducers being 1 cm above the floor, no interference of the boundary layer on the measurements is expected. Moreover, the mean boundary-layer vorticity lies along the ultrasound path, i.e., in the spanwise direction, and therefore it could not contribute to the circulation measurements in an average sense. Measurements of the circulation around the closed path without the wing resulted in values in agreement with the minimum reading of the instrument.

The question of cessation of circulation increase with angle of attack at high α still must be addressed. A potential explanation may be the relative position of the primary vortex core with respect to the measurement plane. The vortex core trajectory is nearly straight and makes angle ϕ with the wing surface and angle ψ with the symmetry plane. As the angle of attack increases, the vortex core trajectory lifts away from the surface and approaches the symmetry plane for both 60- and 70-deg wings. Angle ϕ increases from 4 to 10 deg, whereas ψ decreases from 21 to 13 deg for the 60-deg wing and from 14 to 12 deg for the 70-deg wing. The core trajectory remains independent of Reynolds number.[4] Consequently, the circulation measured by the ultrasound system is less than that present in the plane normal to the vortex core by $\sin\phi \sin\psi$. This product has maximum values less than 4% for the 60-deg wing and less than 2% for the 70-deg wing. These corrections are fairly minor, comparable with the standard deviation of the data, and cannot explain the cessation of circulation growth at high α.

It is instead proposed that the cessation of circulation increase with the angle of attack at high α is a result of the interaction of separated shear layers with the symmetry plane prior to their rolling up. This condition is referred to in the literature as vortex crowding or feeding-sheet interaction. At relatively low angles of attack, the entire vorticity in the separated shear layers gets wrapped into the primary vortex cores. As α increases beyond a certain value, the shear layers containing opposite-sign vorticity from the two leading edges of delta wings impinge on and interact along the symmetry plane before being incorporated into the vortex cores. The interaction of opposite-sign vorticity would tend to reduce the total vorticity present above the wing. In the case of half-delta wings, the separated shear layers would impinge on the floor surface and get dispersed by viscous effects. The feeding-sheet interaction is a direct consequence of the increasing size of the vortex core and the decreasing proximity of the core trajectory to the symmetry plane as the angle of attack is increased.

To ascertain that the observed behavior of circulation with α at high angles of attack is a consequence of feeding-sheet interaction,

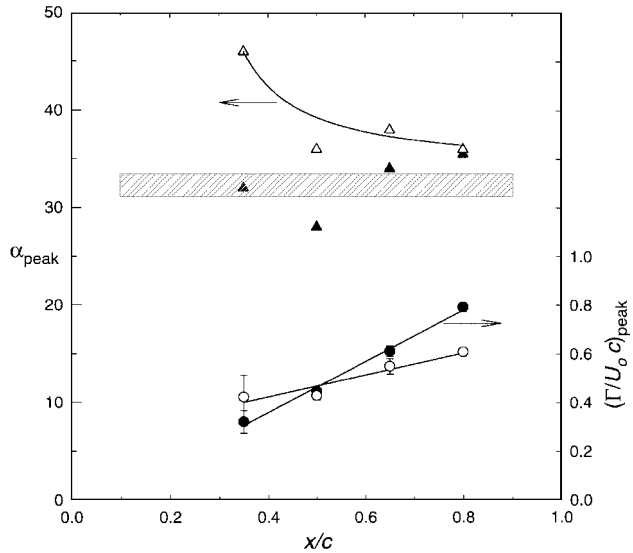

Fig. 9 Peak circulation and the angle of attack at which it was measured as a function of the axial location along the chord. The open and filled symbols refer to 70- and 60-deg delta wings, respectively. The shaded region is the range of angles of attack for which merging of feeding sheets from the two leading edges was observed in Ref. 10 for 60-deg delta wings.

the angles of attack at which the peak circulations were measured are plotted against the chordwise position in Fig. 9. The 70-deg wing data reveal a decreasing trend of peak α with x/c. In other words, the interaction of feeding sheets with the symmetry plane starts from the vicinity of the trailing edge and moves toward the apex as α increases. Flow visualization of Roos and Kegelman[10] employing full-span, sharp-edged, flat-plate, 70-deg sweep delta wings resulted in a similar trend. The visually observed interaction moved from the midchord to the apex when the angle of attack was increased from about 44 to 48 deg. The feeding-sheet interaction for the 60-deg wing was observed to occur over a narrow range of about 3 deg along the entire chord length at $\alpha \cong 33$ deg. This range is shown as the shaded region in Fig. 9. Current measured peak circulations occur at angles of attack roughly consistent with the flow visualization study of Ref. 10. Thus, the interaction of feeding sheets is correlated with the angles of attack at which peak circulations were measured. At all x/c stations, the feeding-sheet interaction was observed at angles of attack beyond those where the vortex bursts; i.e., the interaction was observed only with burst vortices.

The values of peak circulation, also plotted in Fig. 9, increase linearly with x/c for both 60- and 70-deg wings, even though the angles of attack associated with the data are different. The slope, $d\Gamma_{peak}/dx$, is greater for the 60-deg wing data than the 70-deg wing. As implied in Ref. 10, the feeding-sheet interaction, and not the vortex breakdown, is responsible for the stall of delta wings. Current observations of the cessation of circulation increase beyond certain angles of attack corroborate this conjecture. Wentz and Kohlman[20] found the maximum lift coefficient of the 60- and 70-deg delta wings to be at 30 and 34 deg, respectively, in rough agreement with the average angles of attack at peak circulation, α_{peak}, in current observations. Moreover, the softer stall of the 70-deg wing is speculated to be a result of the marching of the feeding-sheet interaction toward the apex, in contrast to the appearance of the interaction almost uniformly along the 60-deg wing.

Last, current measured data can be compared against the model of Hemsch and Luckring[13] for slender wings, which utilizes the Sychev similarity parameter[12] $\tan\varepsilon/\tan\alpha$. The model scales the total circulation at the trailing edge of slender wings with wing geometrical parameters. The model was realized from a power-law fit to the circulation obtained from the numerical results of Smith[23] for slender conical flows and the velocity profiles of Delery et al.[24] in the near wake of a 75-deg delta wing. Visser and Nelson[9] extended the model to correlate the vortex strength above delta wings at any chordwise location. The extended model predicts the circulation, normalized

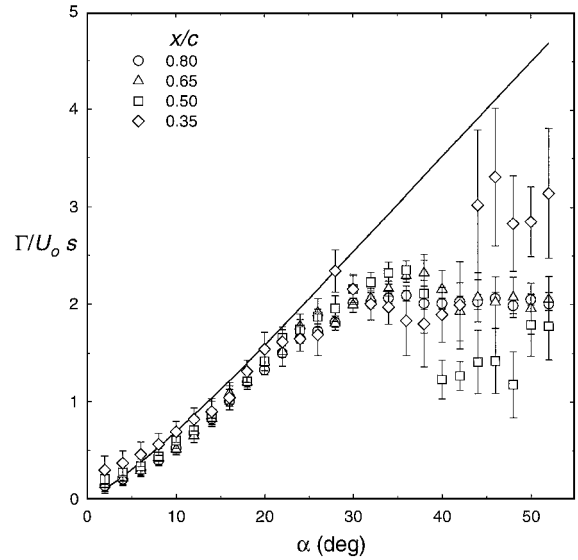

a) 70-deg delta wing

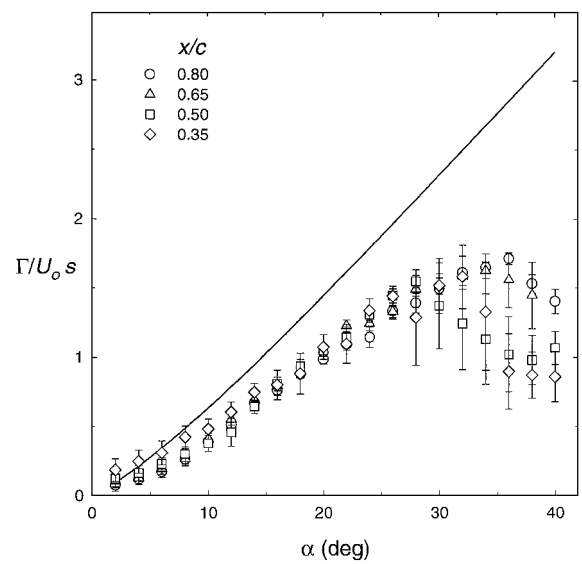

b) 60-deg delta wing

Fig. 10 Variation of circulation, normalized by the local semispan and freestream velocity, with angle of attack. The curve in each plot represents Eq. (4).

by the local semispan s, in terms of the angle of attack and apex half-angle ε as follows:

$$\Gamma/U_o s = A(\sin\alpha)^n(\cos\alpha)^{(1-n)}(\tan\varepsilon)^{(1-n)} \qquad (4)$$

where n was found in Ref. 13 to be 1.2. The proportionality constant A was determined by Visser and Nelson[9] to be 4.63 from a best fit to their data and those of Payne[11] for wing sweep angles of 70 deg and higher. The data of Wentz and McMahon[25] for a 62-deg sweep delta wing appeared to be somewhat less than that predicted by Eq. (4).

The present circulation data were normalized by the local semispan at each measurement station for comparison with the predictions of Eq. (4). The normalized circulation ($\Gamma/U_o s$) data are presented in Fig. 10 for both sweep angles as a function of angle of attack. The normalization by the local semispan collapses current data fairly consistently for angles of attack up to about 30 and 34 deg for the 60- and 70-deg wings, respectively. The consistency in the collapse of the data also confirms the validity of assuming that the negative vorticity of secondary vortex can be counted as a bias error. The 70-deg wing data agree closely with the predictions of Eq. (4) to about 30-deg angle of attack, beyond which the measured circulation settles into a level value of about $2sU_o$. The deviation from the model for the 70-deg delta wing becomes significant beyond about

34 deg, which is consistent with the angle where feeding-sheet interaction starts at the trailing edge. The loss of the collapse of data from various x/c locations also occurs at $\alpha = 34$ deg because of the interaction taking place at different chordwise locations as α increases.

The normalized data for the 60-deg wing in Fig. 10b invariably fall below the prediction of Eq. (4) beyond $\alpha = 10$ deg, even though the data for the four measurement stations collapse up to about 30 deg. Thus, the difference between the data and the model below 30-deg angle of attack cannot be explained by the feeding-sheet interactions discussed earlier. Although the tainting of data by the circulation of the secondary vortex can be a factor, the primary agent is believed to be the breakdown of the fundamental assumption underlying the model. To be considered a slender wing, $\tan\varepsilon$ has to be much smaller than unity. The 60-deg wing has a half-apex angle of 30 deg, or $\tan\varepsilon = 0.58$, which is not much smaller than unity. On the other hand, $\tan\varepsilon$ for a 70-deg wing is only 0.36. The data of Wentz and McMahon[25] for a 62-deg sweep delta wing also fall about 35% below the predictions of Eq. (4), in agreement with current data.

The model in Eq. (4) thus appears to provide a good prediction of the primary vortex strength for low-aspect-ratio wings ($\Lambda \geq 70$ deg) below angles of attack that result in feeding-sheet interaction. For higher-aspect-ratio wings, the model overestimates the primary vortex circulation. Vortex crowding causes the model to severely overstate the circulation, by as much as a factor of two, at the highest angles of attack studied here.

Conclusions

A novel ultrasound system was utilized for the investigation of delta-wing vortex circulation. The ultrasound method is comparatively easy to implement and is nonintrusive to the primary vortex. The measurements were conducted at four uniformly spaced stations along the chord between $0.35c$ and $0.80c$ on two thin flat-plate delta wings with sweep angles of 60 and 70 deg. Circulation increased monotonically with α for both sweep angles until it reached a maximum value, beyond which the total circulation decreased or remained nearly level. The maximum value of circulation and the angle at which it arises is correlated with conditions resulting in feeding-sheet interaction on the symmetry plane. The angle of attack at maximum circulation was about 33 ± 3 deg for the 60-deg wing, and it varied from 36 to 46 deg for the 70-deg wing. These ranges are consistent with previous visual observations of vortex crowding on full-span delta wings.

At any angle of attack, circulation increased linearly with chordwise location along the wing for conditions without feeding-sheet interaction. The rate of circulation increase along the wing $d\Gamma/dx$ increased with α for both sweep angles and was larger for the 60-deg wing. Normalizing the measured circulation by the freestream velocity and local semispan collapsed the data between $0.35 \leq x/c \leq 0.80$ at angles of attack prior to the appearance of vortex crowding. The circulation data for the 70-deg wing agree closely with the model proposed by Hemsch and Luckring[13] up to α_{peak}. The measured data for the 60-deg wing are consistently smaller than the values predicted by the model. Breakdown of the slenderness requirement appears to be the reason for this discrepancy. Thus, as long as the flow can be regarded as a conical flow, i.e., thin wings with high sweep angles, the model predictions are accurate. For low sweep angles or thick wings, the model overestimates the circulation. Interaction of the feeding sheets on the symmetry plane disrupts the rollup of the primary vortex and invalidates the application of Eq. (4).

Vortex breakdown does not have any direct influence on the behavior of total circulation of delta-wing vortices. Circulation continues to grow unabated along the chord as vortex breakdown travels from the trailing edge to the apex. As the angle of attack increases, the total circulation at any chordwise location also increases, even as vortex breakdown passes through. Although vortex breakdown changes the distribution of the axial vorticity significantly, the emergence of vortex breakdown does not alter the sum of shed vorticity from the leading edge. Accordingly, it can be concluded that vortex breakdown is not the main reason for the stall of delta wings. Instead, the loss of circulation at high angles of attack associated with vortex crowding is proposed to be the cause of delta-wing stall.

Acknowledgment

Discussions with Fred Roos regarding the decrease in circulation are gratefully acknowledged.

References

[1]Gad-el-Hak, M., and Blackwelder, R., "The Discrete Vortices from a Delta Wing," *AIAA Journal*, Vol. 23, No. 6, 1985, pp. 961, 962.

[2]Polhamus, E. C., "A Concept of the Vortex Lift of Sharp-Edge Delta Wings Based on a Leading-Edge Suction Analogy," NASA TN-D-3767, 1966.

[3]Escudier, M., "Vortex Breakdown: Observations and Explanations," *Progress in Aerospace Sciences*, Vol. 25, No. 2, 1988, pp. 189–229.

[4]O'Neil, P. J., Roos, F. W., Kegelman, J. T., Barnett, R. M., and Hawk, J. D., "Investigation of Flow Characteristics of a Developed Vortex," U.S. Naval Air Development Center, Rept. 89114-60, Warminster, PA, May 1989.

[5]Lowson, M. V., and Riley, A. J., "Vortex Breakdown Control by Delta Wing Geometry," *Journal of Aircraft*, Vol. 32, No. 4, 1995, pp. 832–838.

[6]Payne, F. M., Ng, T., T., and Nelson, R. C., "Probe Interference on Measurement of Leading Edge Vortex Flows," *Experiments in Fluids*, Vol. 7, No. 1, 1989, pp. 1–8.

[7]Erickson, G. E., "Water-Tunnel Studies of Leading-Edge Vortices," *Journal of Aircraft*, Vol. 19, No. 6, 1982, pp. 442–448.

[8]Chigier, N. A., "Measurement of Vortex Breakdown over a Delta Wing Using a Laser Anemometer," Nielsen Engineering and Research, Inc., TR 62, June 1974.

[9]Visser, K. D., and Nelson, R. C., "Measurements of Circulation and Vorticity in the Leading Edge Vortex of a Delta Wing," *AIAA Journal*, Vol. 31, No. 1, 1993, pp. 104–111.

[10]Roos, F. W., and Kegelman, J. T., "Recent Explorations of Leading-Edge Vortex Flowfields," *High-Angle-of-Attack Technology Conference*, NASA, 1990, pp. 157–172.

[11]Payne, F. M., "The Structure of Leading Edge Vortex Flows Including Vortex Breakdown," Ph.D. Dissertation, Aerospace and Mechanical Engineering Dept., Univ. of Notre Dame, Notre Dame, IN, May 1987.

[12]Sychev, V. V., "Three Dimensional Hypersonic Gas Flow Past Slender Bodies at High Angles of Attack," *Journal of Applied Mathematics and Mechanics (USSR)*, Vol. 24, Feb. 1960, pp. 296–306.

[13]Hemsch, M. J., and Luckring, J. M., "Connection Between Leading Edge Sweep, Vortex Lift, and Vortex Strength for Delta Wings," *Journal of Aircraft*, Vol. 27, No. 5, 1990, pp. 473–475.

[14]Magness, C., Robinson, O., and Rockwell, D., "Instantaneous Topology of the Unsteady Leading-Edge Vortex at High Angle of Attack," *AIAA Journal*, Vol. 31, No. 8, 1993, pp. 1384–1391.

[15]Schmidt, D. W., "Acoustical Methods for Fast Detection and Measurement of Vortices in Wind Tunnels," *ICIASF Record*, International Congress on Instrumentation and Aerospace Simulation Facility, 1975, pp. 216–228.

[16]Johari, H., and Durgin, W. W., "Direct Measurement of Circulation Using Ultrasonic Methods," *Experiments in Fluids* (to be published).

[17]Genthe, W. K., and Yamamoto, M., "A New Ultrasonic Flowmeter for Flows in Large Conduits and Open Channels," *FLOW: Its Measurement and Control in Science and Industry, Part 2, Flow Measuring Devices*, edited by R. E. Wendt Jr., Vol. 1, 1971, pp. 947–955.

[18]Johari, H., Olinger, D. J., and Fitzpatrick, K. C., "Delta Wing Vortex Control via Recessed Angled Spanwise Blowing," *Journal of Aircraft*, Vol. 32, No. 4, 1995, pp. 804–810.

[19]Moreira, J., "Direct Measurement of Delta Wing Vortex Circulation Using Ultrasound," M.S. Thesis, Mechanical Engineering Dept., Worcester Polytechnic Inst., Worcester, MA, May 1996.

[20]Wentz, W. H., Jr., and Kohlman, D. L., "Vortex Breakdown on Slender Sharp Edged Wings," *Journal of Aircraft*, Vol. 8, No. 3, 1971, pp. 156–161.

[21]Earnshaw, D. M., and Lawford, J. A., "Low-Speed Wind-Tunnel Experiments on a Series of Sharp-Edged Delta Wings," Aeronautical Research Council, Repts. and Memoranda 3424, London, 1964.

[22]Verhaagen, N., and van Ransbeeck, P., "Experimental and Numerical Investigation of the Flow in the Core of a Leading-Edge vortex," AIAA Paper 90-0384, Jan. 1990.

[23]Smith, J. H. B., "Calculations of the Flow over Thick, Conical, Slender Wings with Leading-Edge Separation," Aeronautical Research Council, Repts. and Memoranda 3694, London, March 1971.

[24]Delery, J., Pagan, D., and Solignac, J. L., "On the Breakdown of the Vortex Induced by a Delta Wing," *Colloquium on Vortex Control and Breakdown Behavior* (Baden, Switzerland), 1987, pp. 1–25.

[25]Wentz, W. H., and McMahon, M. C., "Further Experimental Investigations of Delta and Double-Delta Wing Flow Fields at Low Speeds," NASA CR-714, 1967.

A. Plotkin
Associate Editor